Supporting Information

SnS_2/SnS p-n heterojunctions with an accumulation layer for ultrasensitive room-temperature NO_2 detection

Quan Sun,[a] Jiaxin Wang,[a] Juanyuan Hao,*[a,b] Shengliang Zheng,[a] Peng Wan,[a] Tingting Wang,[a] Haitao Fang,[a] You Wang *[a,b]

a. School of Materials Science and Engineering, Harbin Institute of Technology, Harbin 150001, P. R. China.
Email: jyhao@hit.edu.cn; y-wang@hit.edu.cn

b. Key Laboratory of Micro-Systems and Micro-Structures Manufacturing, Ministry of Education, Harbin 150001, P. R. China

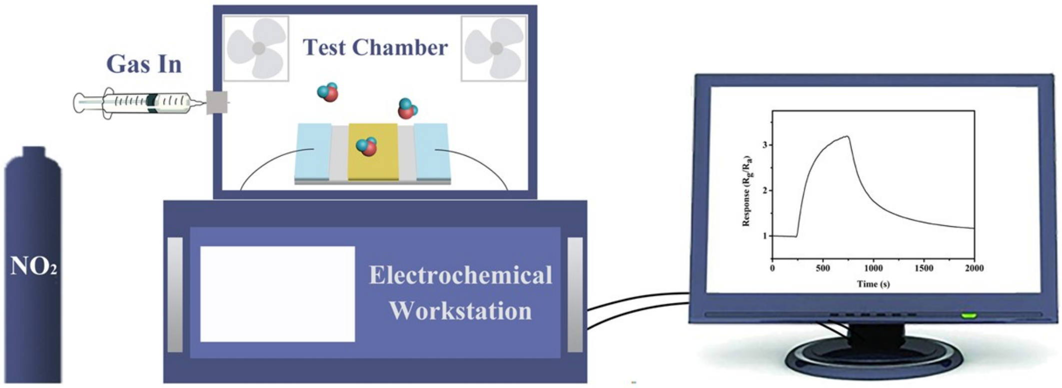

Fig. S1. Schematic diagram of the sensor measurement.

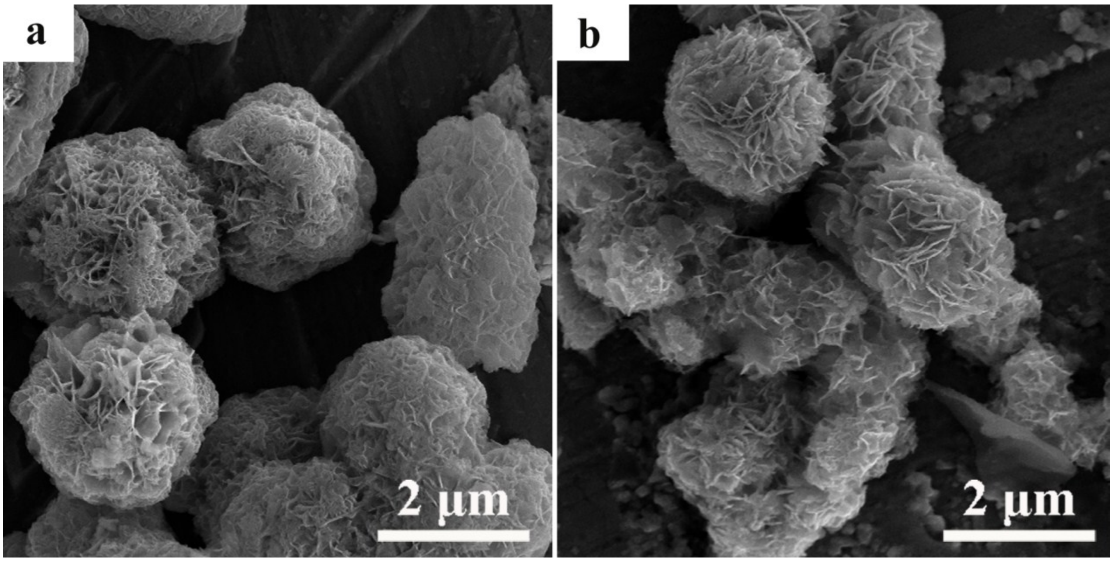

Fig. S2. SEM images of (a) SnS_2/SnS-6 and (b) SnS_2/SnS-1.

Table S1. EDS elemental analysis of SnS_2/SnS-1, SnS_2/SnS-3, and SnS_2/SnS-6.

Sample	S (%)	Sn (%)	S/Sn
SnS_2/SnS-1	55.56	44.44	1.15
SnS_2/SnS-3	61.13	38.87	1.59
SnS_2/SnS-6	63.51	36.49	1.74

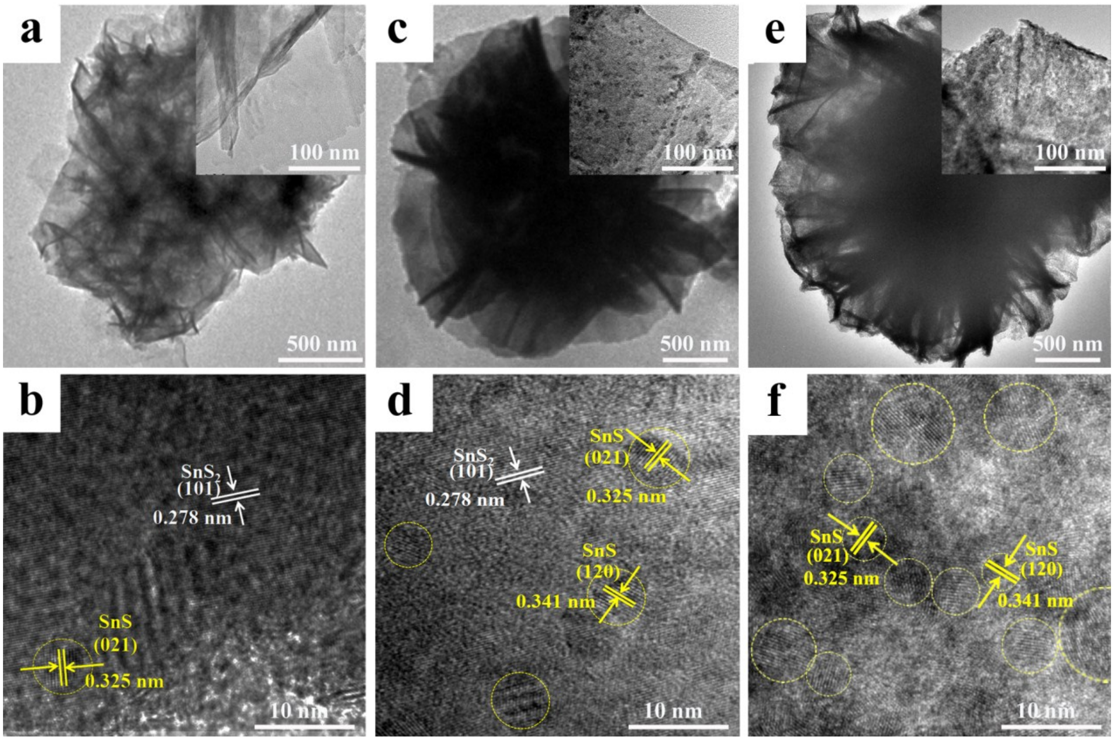

Fig. S3. TEM (top) and HRTEM (bottom) images of SnS_2/SnS heterostructures with different molar ratios of Sn/S in the precursors, (a) (b) SnS_2/SnS-6, (c) (d) SnS_2/SnS-3, and (e) (f) SnS_2/SnS-1.

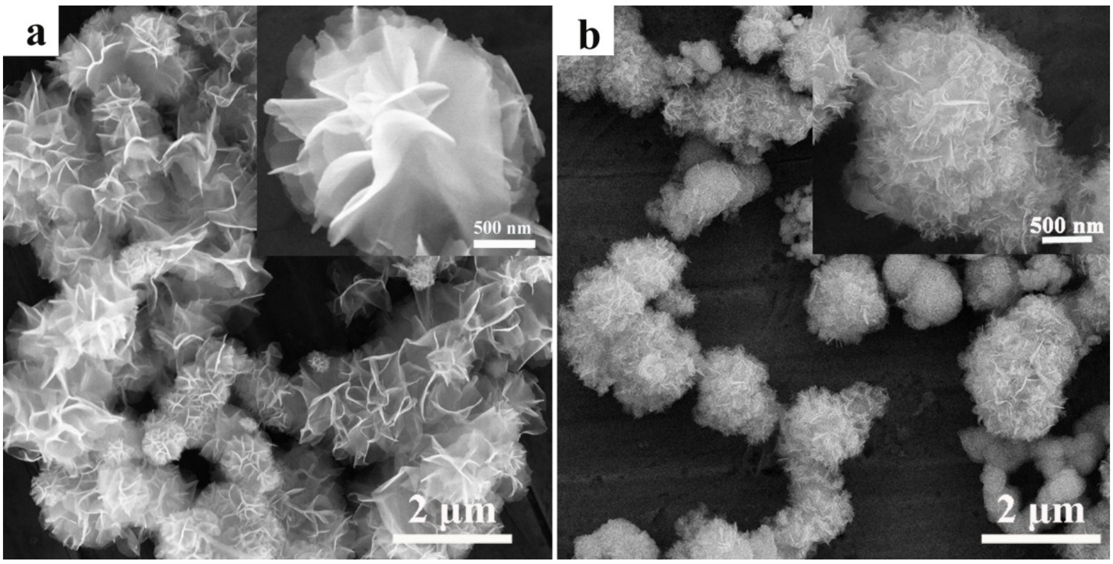

Fig. S4. SEM images of (a) pristine SnS_2 and (b) pristine SnS.

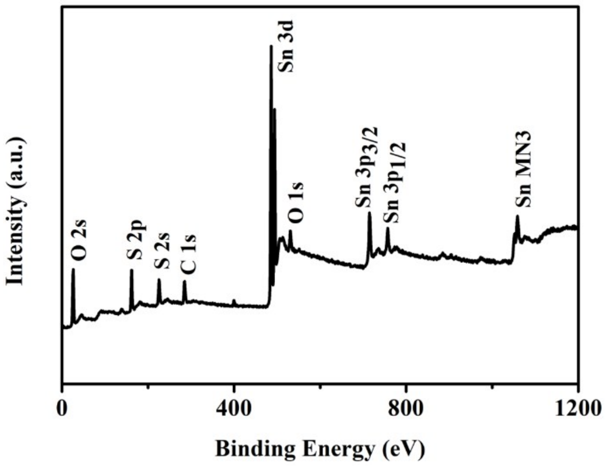

Fig. S5. Survey XPS spectrum of the hierarchical SnS_2/SnS-3 heterostructures.

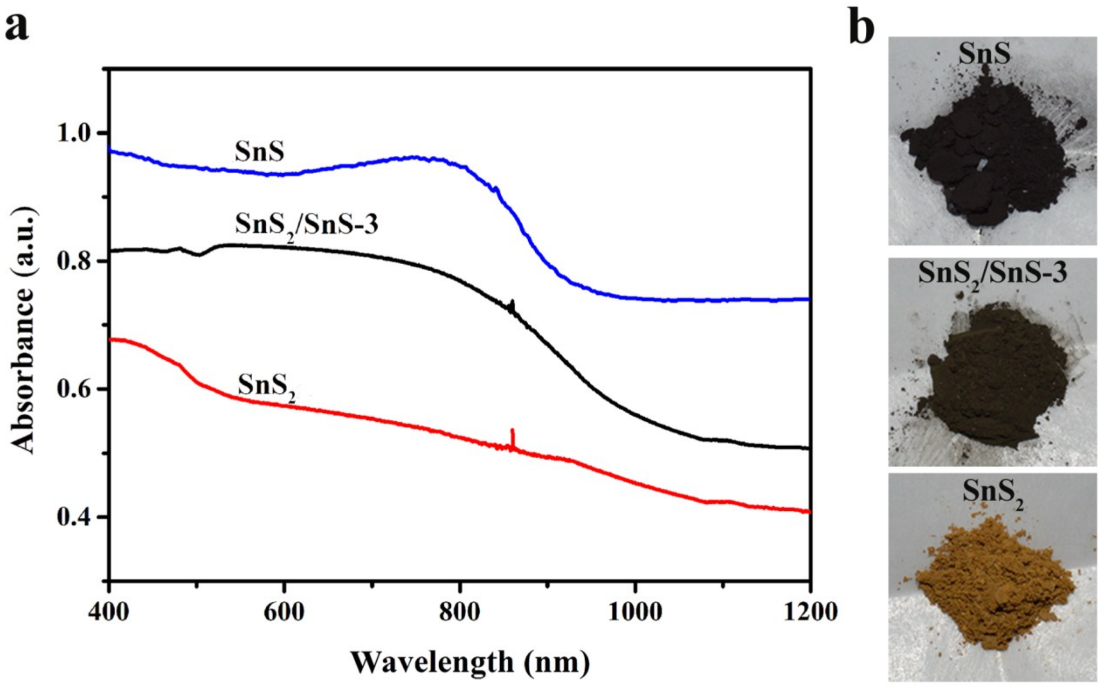

Fig. S6. (a) UV-vis diffuse reflectance spectra (DRS) and (b) digital graphs of SnS, SnS_2/SnS-3, and SnS_2. In Fig. S6a, SnS_2 shows a significant increase in the absorption at wavelengths shorter than 500 nm. While SnS shows a wide absorption range with absorbance peak around 800 nm. For SnS_2/SnS-3, the curve reflects the combination of spectral response of SnS_2 and SnS: it has two absorbance peaks located at around 450 nm and 800 nm, corresponding to the bandgaps of SnS_2 and SnS. Moreover, the heterostructure of SnS_2/SnS-3 is also implied by the sample color (Fig. S6b), which is between yellow of SnS_2 and black of SnS.

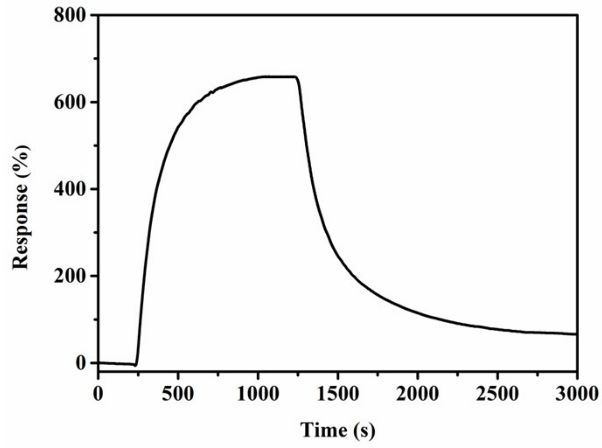

Fig. S7. Dynamic response-recovery curve of the SnS_2/SnS-3 sensor exposure to 4 ppm NO_2 with sensing time of 1000 s.

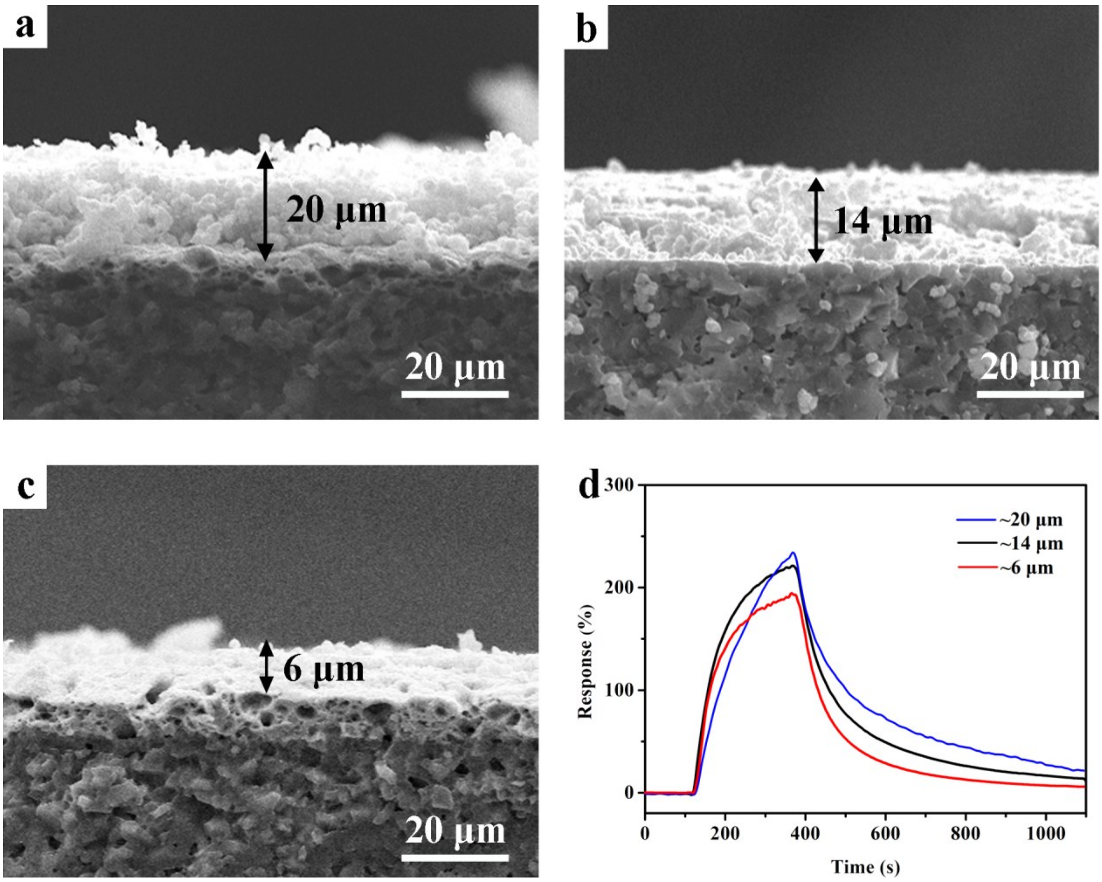

Fig. S8. Cross-sectional-view SEM images of the SnS_2/SnS-3 sensor with different thickness: (a) ~20 µm, (b) ~14 µm, (c) ~6 µm, and their sensing response curves toward 1 ppm NO_2 at room temperature (d).

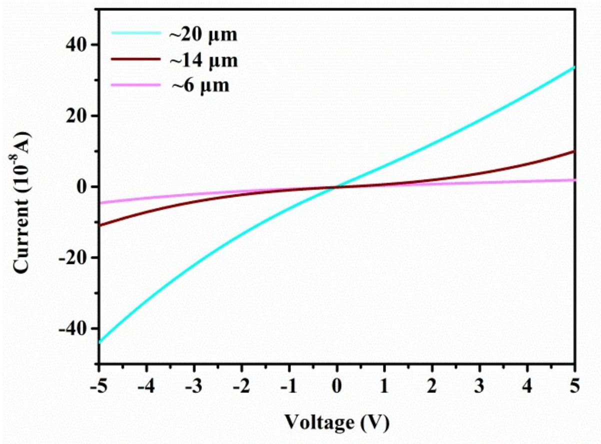

Fig. S9. I-V curve of the SnS_2/SnS-3 sensor with different thickness.

Table S2. The recovery time of the SnS_2/SnS-3 sensor toward various concentrations of NO_2 at room temperature. The recovery time is calculated by the time difference between reaching the final response point and the 90% recovery point.

Conc. (ppm)	**0.125**	**0.25**	**0.5**	**1**	**2**	**4**	**6**	**8**
Response time (s)	391	370	375	300	328	365	369	373
Recovery time (s)	1567	1579	1590	1379	1332	1216	1065	997

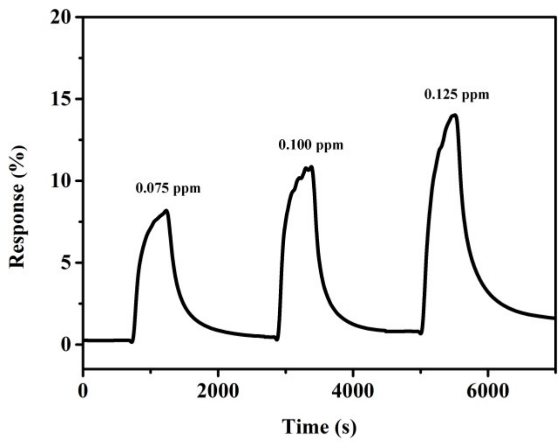

Fig. S10. The response of the SnS_2/SnS-3 sensor to 0.075, 0.100, and 0.125 ppm NO_2 at room temperature.

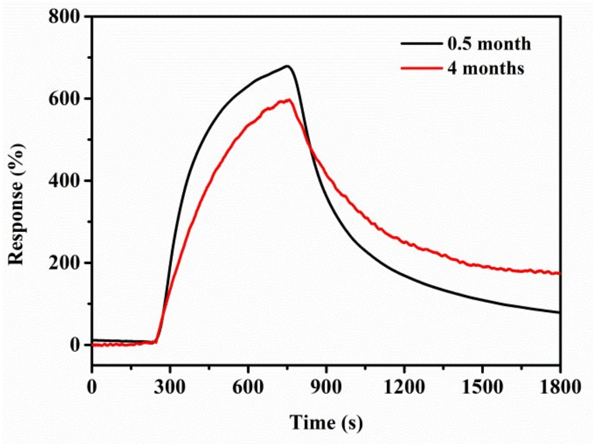

Fig. S11. The response and recovery curve of the SnS_2/SnS-3 sensor after aging 0.5 month and 4 months to 4 ppm NO_2 at room temperature.

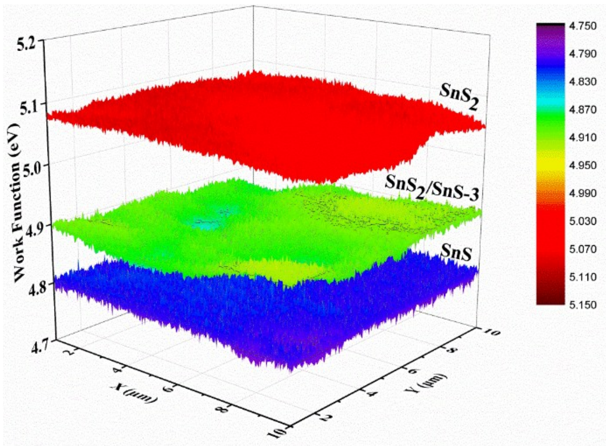

Fig. S12. Work functions of SnS_2 (5.07 eV), SnS/SnS_2-3 (4.89 eV), and SnS (4.79 eV) measured by Kelvin probe based on 218 data points.

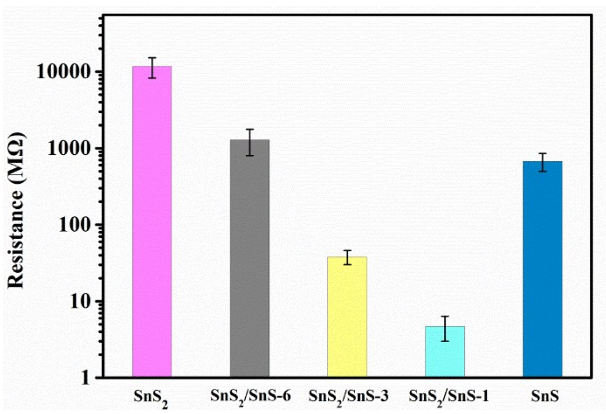

Fig. S13. Working resistance of the SnS_2, SnS_2/SnS-6, SnS_2/SnS-3, SnS_2/SnS-1, and SnS sensors.

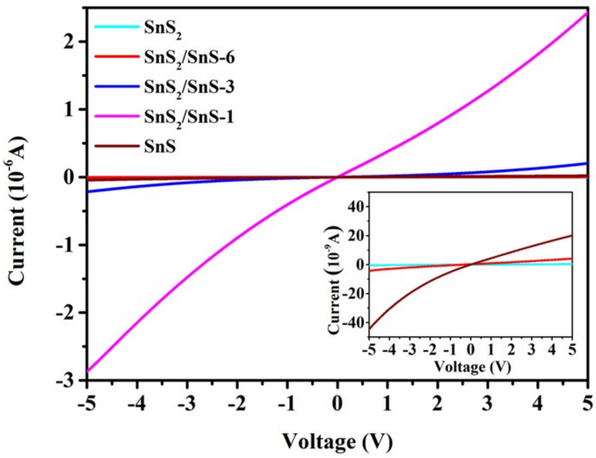

Fig. S14. *I-V* curve of the pristine SnS_2, SnS_2/SnS-6, SnS_2/SnS-3, SnS_2/SnS-1, and pristine SnS sensors.

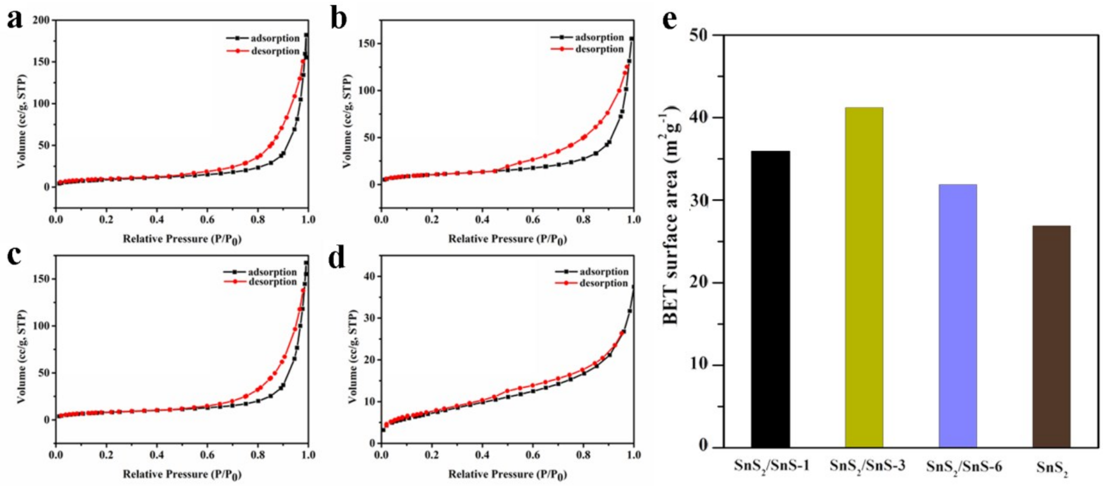

Fig. S15. Nitrogen adsorption/desorption isotherms of (a) SnS_2/SnS-1, (b) SnS_2/SnS-3, (c) SnS_2/SnS-6, (d) pristine SnS_2, and (e) their corresponding Brunauer-Emmett-Teller (BET) surface area.